Available online at www.sciencedirect.com

ScienceDirect

Procedia Engineering 2 (2010) 1829–1837

Procedia Engineering

www.elsevier.com/locate/procedia

Fatigue 2010

Experimental and numerical investigations of fatigue crack growth in various specimen geometries

Igor Varfolomeev*, Michael Luke, Sergii Moroz

Fraunhofer Institute for Mechanics of Materials IWM, Wöhlerstr. 11, 79108 Freiburg, Germany

Received 8 March 2010; revised 10 March 2010; accepted 15 March 2010

Abstract

This paper presents some experimental results demonstrating the geometry dependence of fatigue crack growth (FCG) curves for the steel EA4T (25CrMo4). The experimental results exhibit considerable differences in FCG rates measured on M(T) and C(T) standard specimens, as well as specimens with surface cracks. To explore the possibility of an analytical description of these effects, a numerical analysis is applied to simulate crack growth behaviour for the M(T) and C(T) geometries with special emphasis put on modelling plasticity induced crack closure. The analysis results provide an adequate qualitative description of the crack propagation in different specimens and suggest an explanation for the difference in respective FCG data. On the other hand, a re-evaluation of the experimental results is undertaken to explore a correlation between crack growth rates and the amount of crack tip yielding, with the latter being quantified in terms of the plasticity parameter L_r of the failure assessment diagram. Such an analysis demonstrates that, even though small scale yielding conditions prevail at the crack tip, the FCG curves for individual specimens depend upon and can be arranged according to the plasticity level. Thus, the results suggest that engineering calculations of fatigue crack propagation can be facilitated by incorporating the L_r factor as an additional influencing parameter to take into account the geometry and load effects on FCG rates.

Keywords: Fatigue crack growth; surface cracks; crack tip constraint; ligament yielding

1. Introduction

Fatigue crack growth (FCG) curves measured on standard specimens are often regarded as material specific data. Consequently, engineering analyses of fatigue crack propagation are usually performed using empirically established correlations between the FCG rate, da/dN, and the stress intensity factor range, ΔK, as originally suggested by Paris and Erdogan [1]. The validity of such an approach is basically restricted to small scaled yielding conditions at the crack tip that implies the similitude of the crack tip fields [2], even though some investigations demonstrate the applicability of da/dN-ΔK curves at high load levels corresponding to extensive plastic deformations at the crack tip [3, 4]. Note, however, that the evaluation of test results in [3, 4] is carried out using an empirically estimated elastic-plastic J-integral as the crack driving force parameter.

* Corresponding author. Tel.: +49-761-5142-210; fax: +49-761-5142-401.
E-mail address: igor.varfolomeev@iwm.fraunhofer.de.

1877-7058
doi:10.1016/j.proeng.2010.03.197

On the other hand, fatigue crack propagation in metallic materials arises from plastic deformations at the crack tip, so that FCG rates are expected to correlate with the extent of material yielding. Since the latter depends on the local state of stress and specifically on the stress triaxiality at the crack tip [5], fatigue crack growth behaviour can depend on the specimen geometry and loading. Indeed, a number of experimental investigations demonstrate this feature [6-9]. In particular, two standard geometries – compact tension C(T) and middle tension M(T) specimens – are shown to produce distinctly different FCG curves, whereas the M(T) data usually reveal higher FCG rates at the same ΔK values [6, 8, 9]. On the contrary, experimental data in [7] demonstrate the opposite trend with a faster crack growth noted for C(T) specimens. As the C(T) and M(T) geometries are known to represent standard specimens with the utmost and the lowest stress triaxiality, respectively [10], attempts have been made to include an appropriate constraint parameter, such as the T-stress, in the description of FCG behaviour. In particular, Hutar et al. [8] suggested to modify the crack driving force in the Paris-Erdogan equation by including an empirical correction term, $\lambda(T/\sigma_0)$, being a function of the ratio of the T-stress to the material yield strength. In various numerical studies, e.g. [11-13], the impact of crack tip constraint on the crack growth behaviour is quantified in terms of the plasticity induced crack closure.

This paper summarizes experimental results on FCG rates in different specimens made of steel 25CrMo4 (material EA4T) used in the manufacturing of railway axles. Additionally to basic data derived on M(T) specimens within the framework of the research project "Safe and economic operation of railway axles" [14], the extended database presented here includes results for C(T) specimens, as well as round bars and a rectangular plate containing semi-elliptical surface cracks. In attempt to explain differences in FCG rates, a numerical analysis is applied to simulate crack propagation in the M(T) and C(T) geometries with a particular emphasis put on modelling plasticity induced crack closure. On the other hand, an alternative evaluation of the experimental results is undertaken to explore a correlation between crack growth rates and the measure of crack tip yielding expressed in terms of the plasticity parameter L_r of the failure assessment diagram (FAD). The results suggest that engineering calculations of fatigue crack propagation can be facilitated by incorporating the L_r factor as an additional influencing parameter to take into account the geometry and load effects on FCG rates.

Nomenclature

a	crack depth for semi-elliptical cracks; characteristic crack size for standard specimens
c	half crack length; characteristic value of crack length for round bars
C(T)	compact tension specimen
da/dN	fatigue crack growth rate
FAD	failure assessment diagram
FCG	fatigue crack growth
K	stress intensity factor (mode I)
L_r	plasticity parameter of FAD
M(T)	middle tension specimen
r	radius of a round bar
R	stress intensity ratio, K_{min}/K_{max}
t	plate thickness; thickness of M(T) or C(T) specimen
W	width of C(T) specimen, half-width of M(T) specimen
ΔK	stress intensity factor range
ΔK_{th}	threshold stress intensity factor rang

2. Fatigue Crack Growth Data

2.1. Reference curves

The material considered in this study is the steel 25CrMo4 (EA4T) with the following mechanical properties: yield strength $R_{p0.2} = 552$ MPa, ultimate strength $R_m = 689$ MPa, elongation at fracture $A_5 = 20.6\%$, contraction at fracture $Z = 70.4\%$, the Charpy energy $C_V = 132.1$ J. The above data refer to the room temperature (RT) and represent average values derived from three test specimens.

Reference fatigue crack growth curves for the EA4T steel have experimentally been obtained in [14] at RT using M(T) specimens with the cross-section of $2W \times t = 24 \times 10$ mm². Figure 1 shows the FCG data for two stress ratios $R = -1$ and $R = 0.1$. Table 1 lists the threshold stress intensity factor ranges ΔK_{th}, as well as the constants C and m of the Paris-Erdogan equation [1]

$$\frac{da}{dN} = C\Delta K^m \tag{1}$$

derived based on the experimental data in [14].

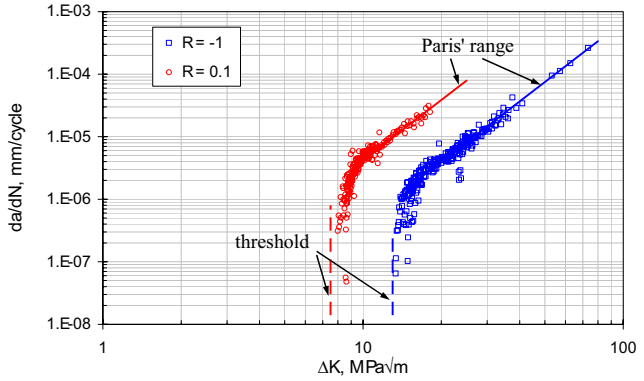

Fig. 1. Reference FCG data for the EA4T material: M(T) specimens, $R = -1$ and $R = 0.1$

Table 1. Threshold stress intensity factor range and parameters of the Paris-Erdogan equation for the EA4T steel, M(T) specimens (units MPa√m for ΔK, mm/cycle for da/dN)

Stress ratio, R	ΔK_{th}, MPa√m	Parameters of Eq. (1)	
		C	m
-1	13	2.74×10^{-10}	3.2
0.1	7.5	2.65×10^{-9}	3.2

2.2. FCG data for various specimens

Additional experimental investigations were performed in [9] to involve various specimen types with different crack tip constraints. Supplementary to the M(T) geometry, seven C(T) 25 standard specimens were tested at $R = 0.1$. Furthermore, three specimens containing semi-elliptical surface cracks – two round bars with the radius $r = 50$ mm (designated as BP1 and BP2) and a rectangular plate with the thickness $t = 30$ mm and the width

$2W$ = 140 mm (designated as BP3) – were included in that study. The surface cracked specimens were subjected to plane bending with the stress ratio R = 0.1.

Figure 2 shows fracture surfaces of the round bar BP2 and the rectangular plate BP3. The crack size and shape were successively monitored by producing beach marks. Apparently, the crack shape is adequately described by semi-elliptical models, Fig. 2, with a and $2c$ referred to as the crack depth and length, respectively. For the round bar, the parameter $2c$ represents a fictitious crack length measured between the intersection points of the extrapolated elliptic contour with the horizontal axis y, Fig. 2a. Upon the crack size measurements, the evaluation of test results for the C(T), round bar and rectangular specimens was performed using stress intensity factor solutions according to [15], [16] and [17], respectively.

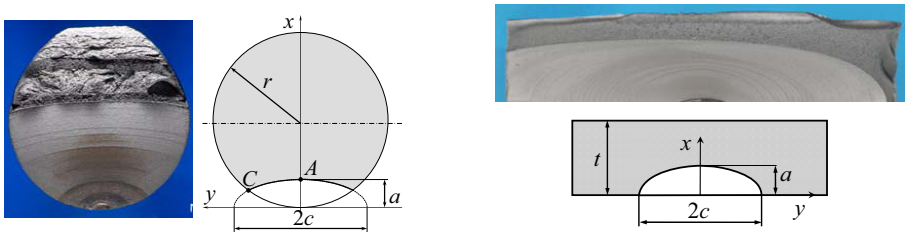

(a) (b)

Fig. 2. Fracture surfaces with beach marks and appropriate crack models: a) round bar BP2; b) rectangular plate BP3

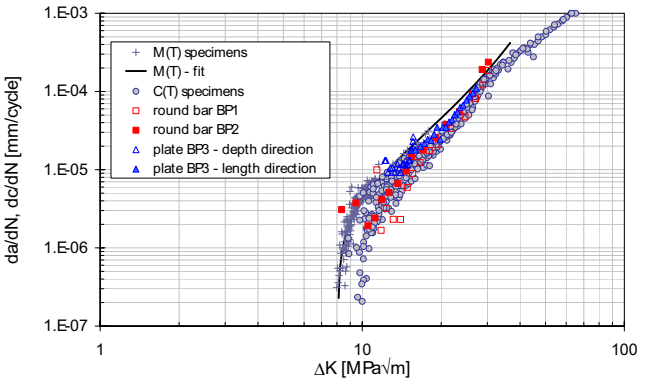

Fig. 3. FCG rates for different specimens: EA4T material, R = 0.1

Fatigue crack growth data for the M(T), C(T) and surface cracked specimens at R = 0.1 are summarized in Fig. 3. To better distinguish between the M(T) and the other specimen types, the M(T) data are smooth curve fitted. The fitting curve is then extrapolated beyond the upper range of da/dN-ΔK data for M(T) specimens corresponding to approximately ΔK = 18 MPa√m or $da/dN = 3.3\times10^{-5}$ mm/cycle. As a rule, FCG rates measured on M(T) specimens represent an upper bound to all other specimen geometries. Some exceptions observed for the initial stage of crack propagation in the rectangular plate and round bars can be attributed to load history effects at precracking, as well as to errors in measuring the crack geometry immediately after precracking.

Within the range of ΔK = 12 to 20 MPa√m, FCG rates for C(T) specimens are on average about twice lower than for M(T) specimens, which finding is in a good agreement with the experimental results of [6, 8]. The data for

surface cracked specimens are mostly allocated between the reference M(T) curve and the lower bound for C(T) specimens. At crack growth rates below some 3×10^{-6} mm/cycle, the round bar data follow the C(T) curve exhibiting a slightly higher ΔK_{th} value, as compared to that measured in M(T) tests [14].

3. Numerical Modelling of Crack Closure

The numerical study reported in this section is focused on the difference in the crack growth behaviour for M(T) and C(T) specimens. The FCG rate assumed in the analysis is 3.3×10^{-5} mm/cycle corresponding to the Paris range of the FCG curves in Fig. 3. The corresponding stress intensity factor ranges are ΔK = 18 MPa√m and 21.6 MPa√m for the M(T) and C(T) specimens, respectively.

The finite-element (FE) models employed in the calculations are shown in Fig. 4. These represent a half of the M(T) and the whole C(T) specimen geometries. The same topology of the crack tip region is used in both models (Fig. 4c). The initial crack tip has a radius of 3 μm; the crack propagation is assumed in the symmetry plane with the total crack extension achieved in the analyses to be equal to 0.2 mm. The corresponding fine mesh region consists of 100 equally spaced elements with the element length of 2 μm. The crack extension is simulated by a consecutive release of nodes in the ligament that belong to the upper and lower halves of the model and are initially connected via multi-point constraints. To achieve the crack growth rate of 3.3×10^{-5} mm/cycle, the node release at the current crack tip is performed after applying 60 load cycles. In all cases, the contact interaction between the opposite crack faces is taken into account. Furthermore, the plane strain condition is assumed.

The numerical calculations were carried out using the ABAQUS FE code [18]. The combined kinematic and isotropic cyclic strain hardening model implemented in [18] was employed with the model parameters selected to fit a cyclic stress versus strain curve available for the material considered.

In contrast to some other investigations, see e.g. [12], no benefit of using the boundary layer formulation was accomplished in this study. As demonstrated in [13], a boundary layer analysis may lead to inaccurate results for specimens subjected to cyclic loading. Possible reasons are the effect of higher order non-singular elastic terms on the plastic deformation at the crack tip, cyclic strain hardening, as well as the crack surface contact. Especially the latter is regarded as a critical aspect leading to the violation of small scale yielding assumptions.

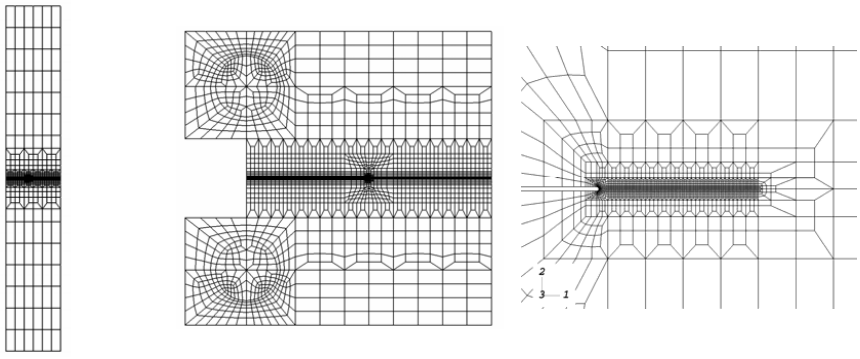

(a) (b) (c)

Figure 4. Finite-element models: a) M(T) specimen, half-model; b) C(T) specimen; c) details of the crack tip region

For a particular crack length, Fig. 5a and Fig. 5b present crack opening profiles in the M(T) and C(T) specimens at various fractions of the maximum load in the cycle. Accordingly, both cracks remain closed for almost 50% of the load cycle. With increasing loading, e.g. at 65% of the maximum value, the crack in the M(T) specimen becomes completely open, while the crack in the C(T) specimen is still partially closed: namely, some portion of the crack faces in the crack tip vicinity, yet excluding the crack tip itself, remains in contact, thus reducing the effective crack driving force.

For the both specimen geometries Fig. 5c compares the crack tip opening displacement (CTOD) defined as the relative displacement of two nodes that belong to the opposite crack faces and are located next to the crack tip. Even though the correctness of such a definition is questioned by the appearance of partial crack closure, especially for the C(T) specimen (Fig. 5b), the results in Fig. 5c allow for an approximate evaluation of the effective stress intensity factor range. The latter is usually defined as

$$\Delta K_{eff} = K_{\max} - K_{op}, \tag{2}$$

with $K_{\max}$ and K_{op} being the linear-elastic stress intensity factors at maximum loading and at the onset of crack opening, respectively. Based on the curves in Fig. 5c, the crack tip opening for the M(T) and C(T) specimens is achieved at some 55% and 62% of the maximum load, or at K_{op} = 11 and 14.9 MPa√m, respectively. This results in ΔK_{eff} = 9 MPa√m for the M(T) specimen and ΔK_{eff} = 9.1 MPa√m for the C(T) specimen, thus suggesting nearly equal crack growth rates for both crack geometries. In contrast, an alternative evaluation of the numerical results based on the contact stress method [11] yields ΔK_{eff} = 9.2 and 9.8 MPa√m for the M(T) and C(T) specimens, respectively [13].

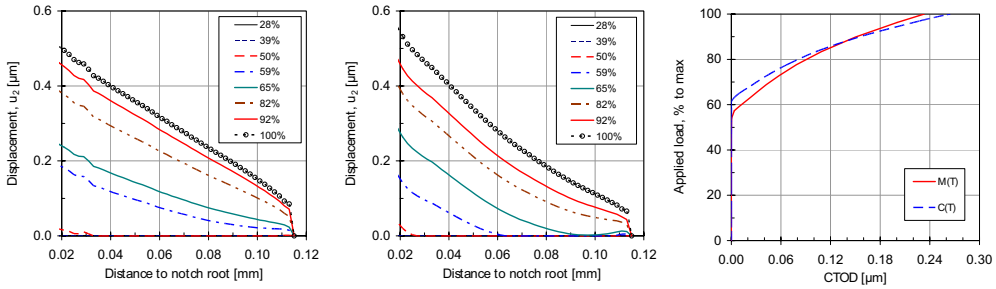

Figure 5. Crack opening profiles for M(T) (a) and C(T) (b) specimens; c) CTOD versus the fraction of maximum load in a cycle

Note that both the CTOD and contact stress based methods are subject to inaccuracies associated with either uncertainties in identifying the onset of crack opening or numerical errors in extracting the contact stresses along the crack faces. Nonetheless, both approaches yield consistent estimates of the effective stress intensity factor range, on the one hand, and provide a rational qualitative and quantitative explanation of the discrepancy between FCG rates for the M(T) and C(T) specimens (Fig. 3), on the other hand.

4. Correlation of FCG Rates with Ligament Yielding

The above experimental and numerical results indicate that the stress triaxiality (constraint) at the crack tip is an important issue influencing FCG behaviour. In accordance with this conclusion, Hutar et al. [8] suggested the *T*-stress, representing a measure of the in-plane crack tip constraint, to be included in the definition of an effective stress intensity factor range. However, being projected onto experimental results of this study, the approach [8] does not explain the fact that FCG curves for the round bars are closely allocated around the lower bound for the C(T) data, although the *T*-stress values for the respective specimens are considerably different [9].

On the other hand, a difference in the stress triaxiality level implies a variation of the size and shape of the crack tip plastic zone [5], so that the analysis of constraint effects is basically consistent with the consideration of material yielding in cracked specimens or components. The measure of ligament yielding can be expressed in terms of the plasticity parameter L_r of the failure assessment diagram, see e.g. [19], representing a normalized reciprocal for the plastic limit load P_L

$$L_r = \frac{P}{P_L} = \frac{\sigma_{ref}}{\sigma_0} \tag{3}$$

with P being the applied load, σ_{ref} and σ_0 the reference stress and the flaw stress, respectively. Note that the crack closure function in [20] involves an empirical term dependent upon the ratio of maximum net stress to the flow stress, σ_{max}/σ_0, which is similar to Eq. (3). Accordingly, the equation developed in [20] predicts accelerated crack propagation at increasing ligament yielding.

In what follows the experimental results given in Fig. 3 are re-evaluated in attempt to explore a possible correlation between FCG rates and the FAD parameter L_r. The values of P_L or L_r for different specimens are estimated using the equations provided in [21-24].

- M(T) specimen, plane strain assumption [21]:

$$P_L = \frac{4(W-a)\sigma_0}{\sqrt{3}} \tag{4}$$

- C(T) specimen [22]:

$$P_L = \frac{2}{\sqrt{3}} Wt\sigma_0 \left(2.572\frac{Q}{W-a} - 1\right)\left(1 - \frac{a}{W}\right)$$
$$Q = \sqrt{(1.052a)^2 + 0.409\left[2a(W-a) + (W-a)^2\right]} - 1.052a \tag{5}$$

- Rectangular bend plate [23]:

$$L_r = \frac{2\sigma_b}{3\sigma_0}\left[1 - \frac{ac}{t(t+c)}\right]^{-0.42} \tag{6}$$

- Round bar under bending stress [24]:

$$L_r = \frac{3\pi}{16}\frac{\sigma_b}{\sigma_0}\left[1.0002 - 3.9927\left(\frac{a_0}{2r}\right)^{1.5} + 5.8491\left(\frac{a_0}{2r}\right)^{2.5} - 2.855\left(\frac{a_0}{2r}\right)^{3}\right]^{-1} \tag{7}$$

The parameter a_0 in Eq. (7) represents the depth of a substitute straight-front crack with the area equal to the area of the original semi-elliptical crack. Further symbols in Eqs (4)-(7) are as follows: W is the half-width or width for M(T) or C(T) specimens, respectively; σ_b is the magnitude of the bending stress.

Equation (6) corresponds with a local limit load representative of ligament yielding at the deepest point of a semi-elliptical crack (crack growth in the depth direction). In contrast, Eq. (7) gives global limit load estimates for a rectangular bar. In case of M(T) and C(T) specimens with through-thickness cracks, Eqs (4) and (5) can be regarded as both local and global solutions.

The plot of the FAD parameter L_r estimated at maximum loading in a cycle versus the stress intensity factor range is given in Fig. 6. Four specimen types considered in this study are included in Fig. 6; individual points correspond with those plotted in the fatigue crack growth diagram, Fig. 3. Several common features can be concluded when comparing the L_r-ΔK and da/dN-ΔK diagrams:

- In both plots, M(T) and C(T) specimens yield overall upper and lower bounds, respectively; some exceptions mentioned for the round bars in the near-threshold regime are likely due to inaccuracies of measuring the crack size and shape immediately after precracking.
- A considerable data scatter for the C(T) specimens is reproduced in both Fig. 3 and Fig. 6.
- Data for individual specimens are allocated according to the level of the net section stress. A notable scatter is found only for those C(T) specimens which were tested under decreasing load in the near-threshold regime.
- The relative position of the data points for two types of the surface cracked specimens with respect to each other, as well as to the M(T) and C(T) curves is consistent in both diagrams.

The interpretation of the experimental results suggested in Fig. 6 confirms that the crack tip and/or ligament plasticity affects fatigue crack growth rates, even though the small scale yielding conditions prevail at the crack tip. Hence, the transferability of test results from standard specimens to components can be facilitated by taking into account plasticity effects. Note, however, that such an assessment requires a consistent definition of the plasticity parameter. For instance, as discussed above, Eq. (6) is valid for L_r estimates at the deepest point of a semi-elliptical crack. Being applied to the surface point (specimen BP3, length direction), Eq. (6) seems to produce improper results demonstrating a different trend in comparison to all other data.

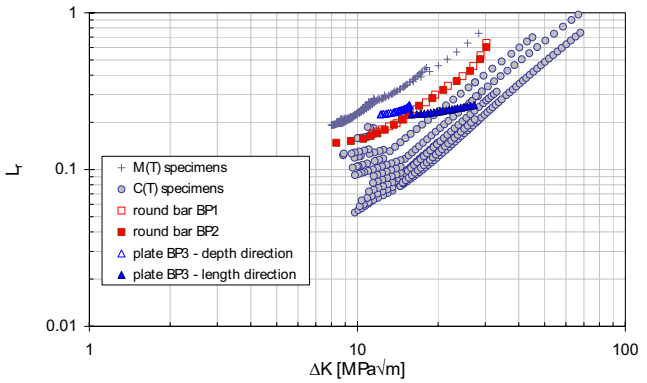

Fig. 6. Relation between the stress intensity factor range and the FAD parameter L_r

5. Conclusions

Experimental results on fatigue crack propagation presented in the paper demonstrate the dependence of FCG curves upon the specimen geometry. Among specimen types considered in this study, M(T) and C(T) specimens yield the upper and lower bounds of FCG rates, respectively. This difference can reasonably be explained by means of a numerical simulation of fatigue crack growth, taking into consideration the plasticity induced crack closure. However, such an approach is rather problematical in case of the assessment of cracked components.

An alternative evaluation of the experimental results revealed a correlation between crack growth rates and the measure of ligament yielding expressed in terms of the plasticity parameter L_r of the failure assessment diagram. The results suggest that engineering calculations of fatigue crack propagation can be facilitated by incorporating the L_r factor as an additional influencing parameter to take into account the geometry and load effects on FCG rates.

References

[1] Paris PC, Erdogan F. A critical analysis of crack propagation laws. Trans. ASME, J Basic Engng 1963;85:528–34.

[2] Anderson TL. Fracture Mechanics: Fundamentals and Applications. 3rd edition. Boca Raton: CRC Press, Taylor & Francis Group; 2005.

[3] Dowling NE, Begley JA. Fatigue crack growth during gross plasticity and J-integral. In: Mechanics of Crack Growth, ASTM STP 590. American Society for Testing and Materials; 1976. p. 82-103.

[4] Brose WR, Dowling NE. Size effects on the fatigue crack growth rate of type 304 stainless steel. In: Landes JD, Begley JA, Clarke GA, editors. Elastic-Plastic Fracture, ASTM STP 668. American Society for Testing and Materials; 1979. p. 720-35.

[5] Larsson SG, Carlsson AJ. Influence of non-singular stress terms and specimen geometry on small-scale yielding at crack tips in elastic–plastic materials. J Mech Phys Solids 1973;21:263–77.

[6] Vecchio RS, Crompton JS, Hertzberg RW. The influence of specimen geometry on near threshold fatigue crack growth. Fatigue Fract Engng Mater Struct 1987;10:333-42.

[7] Tong J. T-stress and its implications for crack growth. Engng Fract Mech 2002;69:1325-37.

[8] Hutar P, Seitl S, Knésl Z. Effect of constraint on fatigue crack propagation near threshold in medium carbon steel. Comp Mat Sci 2006;37:51-7.

[9] Varfolomeev I, Luke M, Burdack M. Investigation of the effect of specimen geometry on fatigue crack growth behaviour. In: 41. Tagung des DVM-Arbeitskreises Bruchvorgänge, Wuppertal, 17-18 February 2007. DVM-Bericht 241, 2009; p. 43-52 (in German).

[10] Sherry AH, France CC, Goldthorpe MR. Compendium of T-stress solutions for two and three dimensional cracked geometries. Fatigue Fract Eng Mat Struct 1995;18:141-55.

[11] Solanki K, Daniewicz SR, Newman Jr JC. Finite element modeling of plasticity-induced crack closure with emphasis on geometry and mesh refinement effects. Engng Fract Mech 2003;70:1475-89.

[12] Roychowdhury S, Dodds Jr RH. A numerical investigation of 3-D small-scale yielding fatigue crack growth. Engng Fract Mech 2003;70:2363-83.

[13] Varfolomeev I, Moroz S. Numerical investigation of constraint effects on fatigue crack propagation. In: Int. Conf. Crack Paths (CP 2009), Vicenza (Italy), 23-25 Sept. 2009; p. 977-84.

[14] Luke M, Varfolomeev I, Lütkepohl K, Esderts A. Fracture mechanics assessment of railway axles: Experimental characterization and computation. Engng Fail Anal 2010;17:617-23.

[15] ASTM E 647-08: Standard Test Method for Measurement of Fatigue Crack Growth Rates. West Conshohocken, PA: ASTM International; 2009.

[16] Varfolomeev I, Burdack M, Luke M. Fracture mechanics as a tool for specifying inspection intervals of railway axles (Part 2). In: 39. Tagung des DVM-Arbeitskreises Bruchvorgänge, Dresden, 13-14 February 2007. DVM-Bericht 239, 2007; p. 33-42 (in German).

[17] Wang X, Lambert SB. Local weight functions for semi-elliptical surface cracks in finite thickness plates. Theor Appl Fract Mech 1995;23:199-208.

[18] ABAQUS Standard, Version 6.7. User's Manual. Dassault Systèmes; 2007.

[19] FITNET: Fitness-for-Service (FFS) Procedure. Kocak M et al. (Eds). Geesthacht: GKSS Research Centre; 2008.

[20] Newman Jr JC. A crack opening stress equation for fatigue crack growth. Int J Fract 1984;24:R131-5.

[21] Kumar V, German MD, Shih CF. An engineering approach for elastic-plastic fracture analysis. GE-EPRI Report NP-1931, July 1981.

[22] Hu JM, Albrecht P. Limit load solution and loading behaviour of C(T) fracture specimen. Int J Fract 1991;52:19-45.

[23] Sattari-Far I, Dillström P, Local limit load solution for surface cracks in plates and cylinders using finite element analysis. Int J Press Ves Piping 2004;81:57-66.

[24] API 579-1/ASME FFS-1 2007 Fitness-For-Service. Washington, D.C.: American Petroleum Institute; 2007.